Numerical modeling of the airflow around a forest edge using LiDAR-derived forest heigths

Boudreault, Louis-Etienne; Dellwik, Ebba; Bechmann, Andreas; Sørensen, Niels N.; Sogachev, Andrey

Publication date:
2012

Numerical simulation of the air flow around a forest edge using LiDAR-derived forest heights

Louis-Étienne Boudreault, Ebba Dellwik, Andreas Bechmann, Niels N. Sørensen, Andrey Sogachev
DTU Wind Energy, Technical University of Denmark
Frederiksborgvej 399, DK-4000 Roskilde, Denmark
Email: lbou@dtu.dk

Keywords: Wind turbine siting, Computational fluid dynamics, Forest canopy flow, Light detection and ranging, Digital elevation model.

ABSTRACT

A 3D methodology to quantify the effect of forests on the mean wind flow field is presented. The methodology is based on the treatment of forest raw data of light detection and ranging (LiDAR) scans, and a computational fluid dynamics (CFD) method based on a Reynolds-averaged Navier-Stokes (RaNS) approach using the $k-\varepsilon$ turbulence model with a corresponding canopy model. The example site investigated is a forest edge located on the Falster island in Denmark, where a measurement campaign was conducted. The LiDAR scans are used in order to obtain the forest heights, which served as input to the numerical CFD model. A sensitivity analysis with regards to the resolution of the structured forest height grid obtained from the implemented digital elevation model (DEM) was carried out. CFD calculations were conducted with the forest height grid taken as input and the complete methodology results are finally briefly compared to the wind measurements of the site with regards to the calculated wind field prediction accuracy.

INTRODUCTION

The wind flow field at a forest edge is complex and challenging to reproduce numerically. This flow case is therefore a good validation test for the development of a general numerical wind prediction tool for turbine siting in forested terrain. These type of tools however require accurate inputs for defining the characteristics of the forest (e.g. height and density) and this can be accomplished with the help of a light detection and ranging (LiDAR) device. A LiDAR enables, among other applications, to measure distances from a target with a reflected laser beam. In forestry, the unstructured raw data from LiDAR scans can be processed with a digital elevation model (DEM) to obtain a structured forest height grid. In the context presented here, the focus is to develop such a DEM, and to couple the produced forest height grid from the DEM with a computational fluid dynamics (CFD) flow solver. Here, a parametric function defining the forest density was implemented and used in the CFD flow solver. This innovative methodology allows us to conduct efficient and practical predictions of the wind flow field in forested environments. Different interpolation techniques within the proposed DEM using a local binning algorithm [1, 2] will first be evaluated with regards to the sensitivity of the forest height grid resolution. A best interpolation method will then be identified and CFD calculations will be conducted with the forest height grid produced from the best method. Finally, the CFD results using the complete methodology will be compared and validated against a full scale experiment, where wind measurements were taken near and within a forest edge. The atmosphere is considered as neutrally stratified and the effect of the Coriolis force is neglected.

METHODOLOGY

The Falster forest edge experiment

The Falster forest edge is located on the Falster island in a mixed agricultural-forested area as is shown in Figure 1. The site is mainly populated with tall European

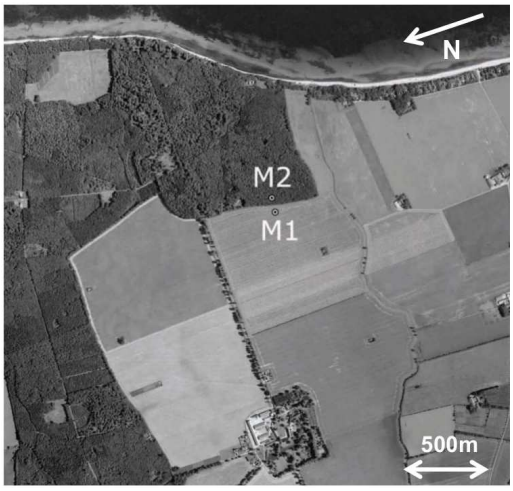

Figure 1: Aerial photograph of the site of interest and its surroundings. The abbreviations M1 and M2 indicate the locations of Mast 1 and Mast 2.

Table 1: Description of the site masts.

Mast	M1	M2
Coordinates (UTM 32N)	6072663.7N 695273.1E	6072643.8N 695343.1E
Instruments levels	11.9m 20.9m 30.9m 45.9m - - -	6.9m 11.9m 18.9m 24.9m 29.9m 36.9m 45.9m

beech trees. From March to September 2008, a measurement campaign was conducted with two masts instrumented (mostly) with sonic anemometers at different levels (see Table 1). The first mast was located in front of the edge (Mast M1) and the second one was located right past the edge within the forest (Mast M2) and they were distanced by 73m from each other. Note that the details of the experimental measurement methodology, as well as the detailed description of the instrumentation will not be covered here, but is currently subjected to another independent investigation [3]. The $\theta = 285^\circ$ wind direction is considered here and corresponds to the near-perpendicular flow direction oriented towards the forest edge. The region under consideration for which the LiDAR scans were taken is a $1km \times 1km$ area bounded by the lower left $(695000E,\ 6072000N)$ and the upper right $(696000E,\ 6073000N)$ coordinates (UTM32N coordinate system). The neighbouring forested regions located on the north and south part of the area of interest, as well as the sea located on the east part of the domain were considered of negligible influence on the flow solution to be presented. Those areas were therefore omitted in the calculation domain. The aerodynamic roughness length of the upstream part of the forest edge is estimated to be $z_0 = 0.03m$ (open flat terrain) and was also kept at this value as an estimate of the sub-canopy roughness.

LiDAR interpolation

The forest characteristics, here the forest height geometry, can be obtained from a scanning laser as a point cloud, i.e. an unorganised collection of reflection points having a set of *xyz* spatial coordinates. The large volume of data obtained from the scans however requires interpolation prior to the CFD model input and a method is therefore presented in what follows. The classification as vegetation and ground points of the LiDAR raw data was first processed with the open source code MCC-LIDAR[1] which is based on a multiscale curvature algorithm [4]. This algorithm more specifically consists in identifying points exceeding a given positive curvature threshold when interpolating a surface spline based on its neighbouring points,

[1] http://sourceforge.net/apps/trac/mcclidar

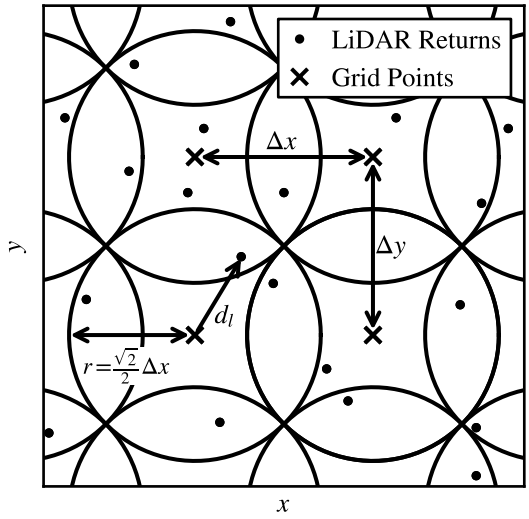

Figure 2: Illustration of the LiDAR point cloud local binning algorithm treatment for a uniformly spaced grid.

and iteratively classify them as vegetation at different domain scales (see [4] for a more complete description). The scale parameter λ and curvature tolerance t used in this process were respectively set as $\lambda = 1.5$ and $t = 0.3$. The two sets of unorganised classified points were further interpolated onto two distinct structured grids using a local binning algorithm [1, 2] in order to reconstruct both the forest and terrain variations. First, this algorithm defines an equally spaced grid, distanced by $\Delta x = \Delta y$ as shown in Figure 2. The LiDAR data is then interpolated on each grid point by generating a circular searching area of radius $r = \sqrt{2}/2 \cdot \Delta x = \sqrt{2}/2 \cdot \Delta y$ so that these areas overlap and cover all the LiDAR returns of a given scanning area (see Figure 2). Statistical approximations can then be used to estimate the elevations in each of the circumvented areas, or so-called *bins*. Different interpolation methods can be defined namely taking the *mean*, *max*, *min* or *inverse distance weighting* (IDW) values of all the LiDAR returns located inside each of the bins around the grid points $Z_{i,j}$ of index i and j as described in [2] as,

$$Z_{i,j}^{mean} = \frac{1}{n}\sum_{l=1}^{n} Z_l \ , \tag{1}$$

$$Z_{i,j}^{max} = max(Z_l), \tag{2}$$

$$Z_{i,j}^{min} = min(Z_l), \tag{3}$$

$$Z_{i,j}^{IDW} = \sum_{l=1}^{n} \frac{Z_l}{d_l^p} \Bigg/ \sum_{l=1}^{n} \frac{1}{d_l^p} \ , \tag{4}$$

where l is the index of the LiDAR returns inside each bins, d is the distance between the returns and the grid point (see Figure 1) and p is the weighting exponent attributed to the distance d. Here, a weighting exponent of $p = 1$ and $p = 2$ will be investigated. The two independent vegetation $Z_{vegetation}$ and ground Z_{ground} grids thus obtained could be

Table 2: $k-\varepsilon$ model constants used

κ	C_μ	σ_k	σ_ε	$C_{\varepsilon 1}$	$C_{\varepsilon 2}$
0.43	0.03	1.0	3.41	1.52	1.83

further subtracted from each other as,

$$Z_{FH} = Z_{vegetation} - Z_{ground}, \tag{5}$$

so that the full horizontal spatial forest height distribution Z_{FH} can be retrieved. For the calculations that will be presented further on, the terrain was approximated as flat and solely the forest height grid Z_{FH} was retained for the CFD input. The minimum value was taken inside the ground bins and this process is believed to filter out the misleading low vegetation points included as ground points that could have subsisted the flagging process of the point cloud mentioned above. Note that empty bins can occur due to insufficient LiDAR ground returns in densely vegetated areas or due to very fine resolution. These empty bins were interpolated by taking the four closest neighbouring grid point values (North-South-East-West), and by approximating the current grid point value using the same interpolation method as the one used for the other grid points as defined by Eqs. (1), (2), (3) and (4). For the site under investigation, a fine grid of 200×200 having a spacing of $\Delta x = \Delta y = 5m$ is used. It is worth mentioning that a LiDAR beam may undergo multiple reflections when a pulse is emitted and reflected. Here, we consider only the first LiDAR returns since we aim to capture the forest height geometry through the reflected pulses from the top of the canopy, and as well as the true ground reflections only.

Numerical model

The standard $k-\varepsilon$ turbulence model with modified constants (referred to in Table 2) implemented in the flow solver EllipSys3D [5, 6] was used. The model was further complemented with a canopy model (see [7] for a complete description) in order to account for the forest drag effect. Here, the drag coefficient serving as input in the canopy model was taken as $C_d = 0.2$ and the leaf area density (*LAD*) was approximated with a parametric function defined as [8],

$$LAD(z) = LAD_m \left(\frac{h-z_m}{h-z}\right)^n \exp\left[n\left(1-\frac{h-z_m}{h-z}\right)\right], \tag{6}$$

where,

$$n = \begin{cases} 6 & \text{if } 0 \le z < z_m, \\ \frac{1}{2} & \text{if } z_m \le z \le h, \end{cases} \tag{7}$$

and h is the forest height at a given location, z the height above the ground and the two parameters $LAD_m = LAD(z_m)$ and z_m are respectively the maximum *LAD* observed at a given height z_m within the forest.

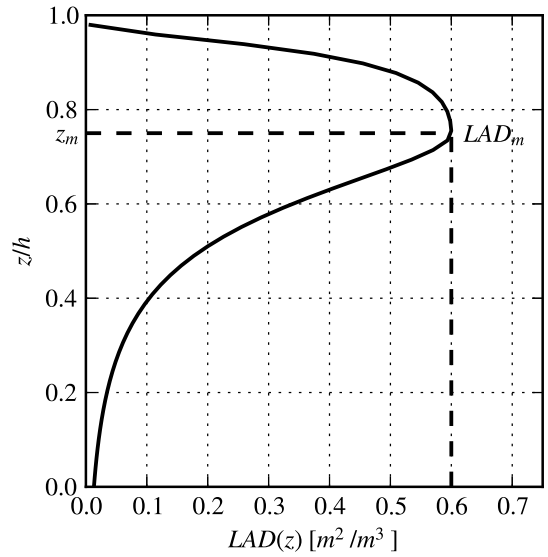

Figure 3: Leaf area density distribution (*LAD*) modeled for the Falster beech tree forest.

For the site investigated, z_m was taken as $z_m = 0.75h$ and $LAD_m = 0.6m^2/m^3$ corresponding roughly to a dense crown tall beech tree forest with a sparse trunk space. The $LAD(z)$ distribution hereby obtained with Eq. (6) is shown in Figure 3. This profile gives an approximate leaf area index[2] (*LAI*) of $LAI = 5.9m^3/m^3$ at the mast M2 location, assuming that the on-field forest inventory estimation of the mean tree height was about $\overline{h} = 25.4m$ around that location. The description of the boundary conditions used in the flow solver can be found in [6]. Note that in this approach, constant shear stress flow solutions of the $k-\varepsilon$ model are assumed as inflow profiles and at the ground boundary (see [6] for a more thorough description). At the top boundary, constant values of velocity u, turbulent kinetic energy k (TKE) and dissipation ε are fixed. The friction velocity u_τ used here as input to these boundary conditions was taken to be,

$$u_\tau = k^{\frac{1}{2}} C_\mu^{\frac{1}{4}} = 0.744m/s, \tag{8}$$

based on the turbulence model constants shown in Table 2 and based on the TKE level observed at the upstream mast M1 ($k/u_{ref}^2 = 0.0432$) at a reference level of $z_{ref} = 30.9m$. The reference velocity at M1 was $u_{ref} = 8.61m/s$ for the wind measurements but was set to $u_{ref} = 10.61m/s$ for the CFD results. The computational grid defined consists in a domain decomposed in multiple blocks where a polar region encompasses a Cartesian region as is shown in Figure 4. This configuration is intended to conduct practical calculations for all the wind directions. The details of the mesh generation can be found in [9]. Here, 2 vertical layers of 96 blocks each of them containing $48 \times 48 \times 48$

[2]The *LAI* being the integrated value of the *LAD* profile trough the canopy depth h as $LAI = \int_0^h LAD(z)dz$.

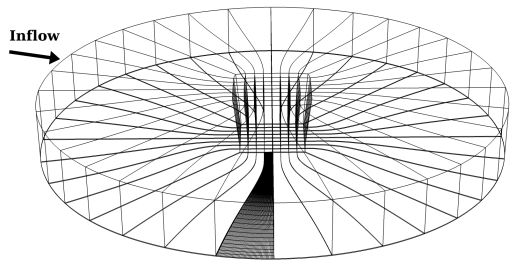

Figure 4: Layout of the multiblock computational grid.

fine grid cells were defined, giving a horizontal $x-y$ spatial grid resolution of $10m$ in the central Cartesian area. The first computational cell height z_1 at the ground is set to be of the same order than the roughness length ($z_1 = 0.03m$) and the above following cells are undergoing a progressive vertical expansion in size. The top boundary was set at a distance of $3172m$ from the ground. The LiDAR forest height grid generated described in the previous section is coupled with the CFD grid by doing a *nearest-neighbour interpolation*. The forest height information serves here as an upper limit below which the cells are undergoing drag forces due the presence of the canopy. The low height vegetation structures below $Z_{FH} < 0.5m$, if present, were filtered out in the calculation process so to avoid problematic sharp unstable local gradients on the near-ground computational cells. The complete aforementioned process was kept the same at each of the levels in the grid sequence of the multigrid flow solver (see [6] for further details). The 3^{rd} order QUICK scheme was used on the advection terms and the solutions were considered converged when the residuals fell under 1×10^{-5}. The kinematic viscosity of the air was assumed to be $\nu = 1.42 \times 10^{-5} m^2/s$.

RESULTS

A nearest-neighbour forest height transect of $1m$ wide passing trough the two mast locations (see Table 1) for the interpolated forest height grid from each of the different presented methods is shown in Figure 5. One can first notice that the mean, IDW1 ($p = 1$) and IDW2 ($p = 2$) methods are predicting similar values of forest heights and these heights are globally lower than the max method over the entire transect. The max values shows less variability but it is not clear which method captures well the gaps and clearings, if physically present they are. In Figure 6, the mean values of forest heights $\overline{h}$ at different grid resolutions for the same transect but over a distance of $137m$ from the forest edge are presented for all the methods. One can first notice that all the methods tend towards the same values as the forest height grid is refined. These heights are compared to the mean value ($\overline{h} = 25.4m$) of on-field samples taken around mast M2 from forest inventory and they show to underestimate this value. It is however important to mention that the forest inventory was realised from the observations of the tallest trees only, and a slight overestimation of this reference value is therefore expected. A more rigorous and methodological on-field forest inventory is in this sense strongly suggested in order to validate the accuracy of the different interpolated forest heights estimates, and as well as to validate the forest height grid resolution required to capture all the local forest features. For the present purpose, the max method nevertheless appeared to be the most appropriate for the site under investigation and is chosen for the calculations to follow.

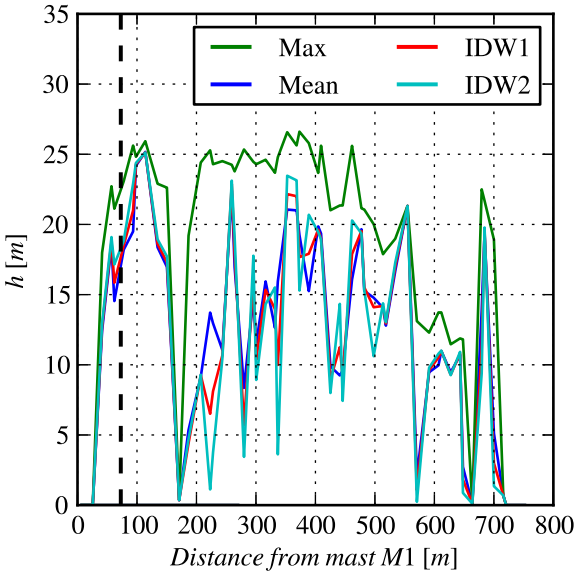

Figure 5: Forest height estimations h on the 200×200 fine forest height grid from the different interpolation methods of the point cloud. IDW1 and IDW2 denotes the inverse distance weighting method with for a weighting exponent of respectively $p = 1$ and $p = 2$. The dashed line indicate the position of mast M2.

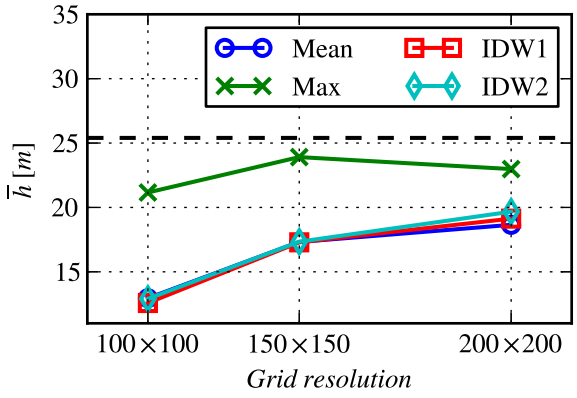

Figure 6: Mean value of forest height $\overline{h}$ computed for different forest height grid resolutions for the transect shown in Fig. 5 going for distance of $137m$ from the forest edge. The dash black line represent a reference value of the forest inventory estimate ($\overline{h} = 25.4m$).

In Figure 7a and 7b, the contours of velocity and a comparison of the predicted near-ground velocity profiles with wind measurements taken during the summer for the projected value of the velocity components onto the 285° direction at the mast M1 and mast M2 locations are respectively presented. The contours in Figure 7a show that an effect of the acceleration of the wind is present over the forest and that a sub-canopy jet penetration is also present, both right past the edge. At mast M1 (Figure 7b), the on-coming upstream profile is in good accordance with the measurements indicating that the inflow conditions are well reproduced. At mast M2 (Figure 7b), the profiles agree well with the measurements in the lower-canopy part but the drag and the speedup effect at either side of the upper part of the canopy are somehow underpredicted. A possible source of discrepancy could be that on-field observations indicated that the edge was densely populated with branches and leaves over its entire height. This physical aspect was not taken into account in the simulated wind field since the leaf area density distribution modeled was in fact resembling a far-edge sparse trunk space tree density distribution. A method for obtaining the local density inside the forest from high resolution LiDAR scans is believed to partly address this problem. It is also worth mentioning that a numerical dependence of the flow solution on the CFD grid resolution is present. This can be attributed in part to the numerical errors due to the discretisation of the domain, but also in part to the possibly sensitive nearest-neighbour interpolation between the the forest height and CFD grids at the different CFD grid levels in the sequence of the multigrid flow solver. This latter influence could be lessened by restricting, with further interpolation, the information of the forest height grid to the same resolution as the actual CFD grid level. These numerical aspects could be of major importance and a more in-depth future sensitivity analysis is strongly suggested to quantify both influences.

CONCLUSION

A 3D methodology for conducting numerical wind flow predictions in forested environments was presented. Different interpolation methods within a DEM for generating a structured forest height grid serving as input to a CFD flow solver from unstructured LiDAR scans raw data were explored. The obtained forest height grids were compared to forest inventory height estimations and a best interpolation method was chosen and coupled with the CFD flow solver. CFD calculations were conducted and compared with wind measurements taken from a full-scale forest edge experiment and the results were in good agreement. From a more general perspective, a closer agreement between the wind measurements and the CFD predictions could be tackled, for example, by introducing the Coriolis force in the CFD flow solver. This further more physical process can have a significant influence for flows over forests. This type of added physical process, and as well as all of the aforementioned possible improvements

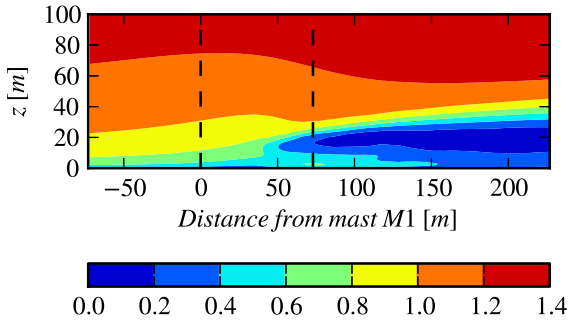

(a) Velocity contours u_{285°/u_{ref}

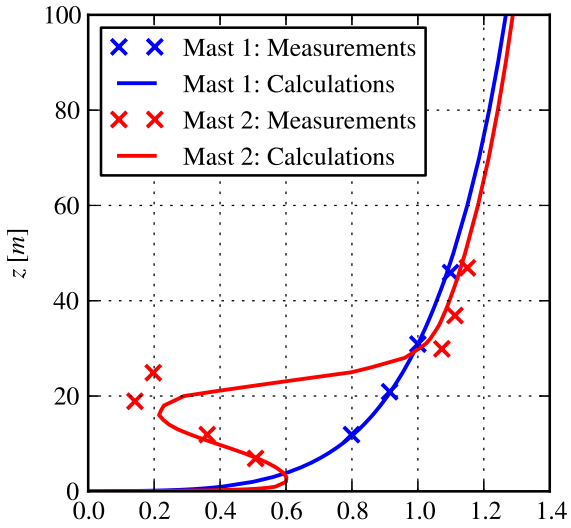

(b) Velocity profiles u_{285°/u_{ref}

Figure 7: (a) Calculated velocity contours for the transect shown in Fig. 5 for the max method (the dashed lines indicate the positions of the masts) and (b) comparison of measured and calculated wind velocities at mast M1 (blue curve) and mast M2 (red curve) locations (see Table 1) for the $\theta = 285^\circ$ flow direction. The reference velocity u_{ref} is taken at mast M1 at $z_{ref} = 30.9m$ for both, wind measurements and calculations.

suggested, could indicate if the further remaining discrepancies are due to insufficient canopy structure description or due to incomplete modeling of the canopy flow process (e.g. turbulence modeling). These questions will be addressed in future work. Nevertheless, the current state of the presented methodology indicate that it is robust and looks promising to be extended with further developments and used as a general tool for predicting the wind field in forested environments.

AKNOWLEDGEMENT

The authors gratefully acknowledge the financial support of Vattenfall and the DSF-“Center for Computational Wind Turbine Aerodynamics and Atmospheric Turbulence”.

REFERENCES

[1] N. El-Sheimy, C. Valeo, and A. Habib. *Digital terrain modeling: acquisition, manipulation, and applications*. Artech House: Boston, MA, 2005.

[2] J. Arrowsmith. Notes on lidar interpolation. `http://lidar.asu.edu/KnowledgeBase/Notes_on_Lidar_interpolation.pdf`.

[3] E. Dellwik. Flow distortion at a dense forest edge. Personal communication, 2012.

[4] J. Evans and T. Hudak. A multiscale curvature algorithm for classifying discrete return lidar in forested environments. *IEEE Transactions on Geoscience and Remote Sensing*, 45(4):1029–1038, 2007.

[5] J. A. Michelsen. Basis3D - a Platform for Development of Multiblock PDE Solvers. Technical report, AFM 92-05, Technical University of Denmark, 1992.

[6] N. N. Sørensen. *General purpose flow solver applied to flow over hills*. PhD thesis, Risø DTU report Risø-R-827(EN), 1995.

[7] A. Sogachev. A note on two-equation closure modelling of canopy flow. *Boundary-Layer Meteorology*, 130(3):423–435, 2009.

[8] B. Lalic and D. Mihailovic. An empirical relation describing leaf-area density inside the forest for environmental modeling. *Journal of Applied Meteorology*, 43(4):641–645, 2004.

[9] N. N. Sørensen. HypGrid2D: a 2D mesh generator. Technical report, Risø DTU report Risø-R-1035(EN), 1998.